metals

MDPI

Article

Investigation of Long-Term Corrosion of CoCrMoW Alloys under Simulated Physiological Conditions

Loredana Preda [1,*], Sorina Alexandra Leau [1], Cristina Donath [1], Elena Ionela Neacsu [1], Monica Elisabeta Maxim [1], Veronica Sătulu [2], Alexandru Paraschiv [3] and Maria Marcu [1,*]

[1] Institute of Physical Chemistry "Ilie Murgulescu", Splaiul Independentei 202, 060021 Bucharest, Romania; sleau@icf.ro (S.A.L.); cdonath@icf.ro (C.D.); eneacsu@icf.ro (E.I.N.); mmaxim@icf.ro (M.E.M.)
[2] National Institute for Laser, Plasma and Radiation Physics, Atomistilor 409, 077125 Magurele, Romania; veronica.satulu@inflpr.ro
[3] COMOTI—Romanian Research Development Institute for Gas Turbines, Iuliu Maniu Bd. 220D, 061126 Bucharest, Romania; alexandru.paraschiv@comoti.ro
* Correspondence: loredana@icf.ro (L.P.); m_marcu@icf.ro (M.M.)

Abstract: The corrosion resistance of two cast CoCr-based alloys with different amounts of chromium and with different alloying elements in the bulk composition of the alloy was assessed. In this study, we investigated the corrosion behavior of Co21Cr8Mo7W and Co29Cr7W by open-circuit potential (OCP), potentiodynamic polarization (PP) and electrochemical impedance spectroscopy (EIS) in 0.1 M phosphate buffer solution (PBS) at 37 °C with long immersion times. After 1000 h of immersion, the corrosion current density (i_{cor}), estimated from anodic polarization tests, was lower for the Co21Cr8Mo7W (i.e., 49 nA cm^{-2}) alloy compared to the Co29Cr7W alloy (180 nA cm^{-2}). As regards the corrosion potential (E_{cor}), a greater value was observed for Co21Cr8Mo7W (i.e., −59 mV vs. Ag/AgCl) compared to Co29Cr7W (i.e., −114 mV vs. Ag/AgCl). Microstructure analysis before and after immersion revealed the formation of a more compact passive film on the Co21Cr8Mo7W alloy, suggesting superior corrosion resistance compared to Co29Cr7W. These findings suggest better corrosion resistance for the film formed on the alloy containing lower amounts of Cr and two alloying elements, Mo and W. These results are promising in terms of medical applications because they open the door to new strategies for obtaining alloys with lower chromium content and with more protective anti-corrosion properties.

Keywords: corrosion; CoCr-based alloy; passive film; biomaterials

Citation: Preda, L.; Leau, S.A.; Donath, C.; Neacsu, E.I.; Maxim, M.E.; Sătulu, V.; Paraschiv, A.; Marcu, M. Investigation of Long-Term Corrosion of CoCrMoW Alloys under Simulated Physiological Conditions. *Metals* **2023**, *13*, 1881. https://doi.org/10.3390/met13111881

Academic Editors: Belén Díaz Fernández, Jianqiang Wang and Branimir N. Grgur

Received: 9 October 2023
Revised: 3 November 2023
Accepted: 9 November 2023
Published: 13 November 2023

1. Introduction

CoCr and titanium alloys are the materials most frequently used in surgical implants and are chiefly used for hard-tissue replacement [1,2]. The use of CoCr-based alloys as biomaterial attracts considerable attention because of their excellent properties, including high corrosion resistance, excellent biocompatibility and good mechanical properties [3,4]. Among the properties required for using these materials in surgical applications, very good corrosion resistance of the alloy is mandatory one [2,3].

The corrosion resistance of these biomaterials is influenced by several factors, such as the alloy itself (e.g., chemical composition, microstructure and surface state), the characteristics of the environment (pH, temperature), and the manufacturing techniques involved [5,6]. For instance, the casting method yields alloys with very good corrosion resistance compared to those obtained by a manufacturing method [7,8]. Concerning the environment, for example, it has been reported that the corrosion resistance of Co28Cr6Mo alloys is drastically reduced when these alloys are tested in NaCl compared to phosphate-buffered saline (PBS) [9]. This behavior is likely associated with the aggressive nature of the chloride ions that most probably attack the protective film formed on the surface, leading to pitting corrosion and finally to dissolution of the film. Conversely, in PBS media, this type of alloy

is less exposed to corrosion attack because during the immersion period, the phosphate ions adsorbed on the surface act as an effective barrier between the alloy and environment [9,10].

As many studies have shown, the corrosion behavior of these types of alloys is significantly influenced by the chemical composition of the alloy as well. Considerable research has been devoted to this subject [11,12]. For example, in the case of the Co29Cr alloy, good resistance to corrosion attack was observed in simulated body fluid (SBF) [13]. This phenomenon can be attributed to the formation of a protective film containing a substantial amount of Cr_2O_3 and small quantities of cobalt oxides [14]. It is generally accepted that the presence of Cr_2O_3 and/or Co $(OH)_3$ species in the film plays a key role in providing good corrosion protection to these CoCr-based alloys. However, on long-time immersion in similar media (e.g., artificial saliva, Ringer's solution and Hank's solution), dissolution processes occur at the alloy/biofluid interface, leading to notable instability in the film [12,14]. In order to address these issues, many approaches have been attempted. Recent data attest that the addition of a small amount of molybdenum to the CoCr alloy leads to the formation of films with notable protective properties. As the electrochemical-corrosion tests evidenced, the Mo itself stabilizes the passive film. These reported data generated new perspectives on methods for obtaining alloys with very good corrosion resistance. Other attempts have been reported over time, including the manufacture of CoCr-based alloys with small amounts of W. In a study of these CoCrW alloys, it was observed that the addition of W does not lead to better stability of the film. Instead, it primarily improves the mechanical properties of the alloy, which does not necessarily improve the corrosion resistance of the material [15].

As a result, in the last few years, molybdenum (Mo) and tungsten (W) have been added as alloying elements to CoCr-based alloys, and promising outcomes have been obtained. In these new alloys, the improved corrosion resistance actually emerges from the synergetic effect of Mo, W and Cr, which promotes the formation of a compact passive film with good stability [11,16,17]. This passive film acts as a barrier between the alloy surface and the biofluid, thus impeding the dissolution of the metallic elements [18]. In other words, Mo and W provide benefits towards passivation and protective role in the breakdown processes, yielding resistance to corrosion attack and thus to the dissolution of the film [17].

Concerning other aspects of using these CoCr-based alloys for medical applications, costs, especially those related to chromium, should be considered. In this respect, new gates were opened by manufacturing CoCr-based alloys with lower Cr content. However, reducing the amount of Cr probably diminishes the corrosion resistance of the material, with undesirable consequences in terms of its use in medical applications. Therefore, in order to reduce the Cr content and at the same time to maintain a good corrosion resistance in CoCr-based alloys, the addition of Mo and W as alloying elements is a valuable option. No data have been reported in the literature about the corrosion behavior of these new types of alloys, i.e., Co Cr MoW, in biofluids. Most frequently, studies investigate the corrosion behavior of CoCr, CoCrMo or CoCrMoW alloys with high amounts of chromium (e.g., 27–30% Chromium) [11,19,20].

In this study, we examined the corrosion behavior of two types of alloys with different concentrations of Cr and with different alloying elements, specifically, W and Mo. These studies are aimed at opening new perspectives on finding strategies for obtaining alloys with low Cr content and with excellent corrosion resistance. For instance, they might offer new perspectives on obtaining other CoCr-based alloys with low chromium content, like CoCr-based alloys that contain other alloying elements such as zirconium or/and niobium or/and copper. Another goal of this research work was to elucidate the role played by alloying elements in the corrosion behavior of these alloys and to offer new information about the significant role of Mo in the corrosion performance of these alloys.

Thus, the corrosion behaviors of two types of alloys after a long period of immersion, i.e., 1000 h, were studied in PBS solution by electrochemical methods (i.e., open-circuit potential (OCP), potentiodynamic polarization (PP) and electrochemical impedance spec-

troscopy (EIS)). The first alloy, labeled Co29Cr7W, contains a high amount of Cr (29% Cr) and contains W as the alloying element, whereas the second one, labeled Co21Cr8Mo7W, contains a lower amount of Cr (21%) and contains Mo and W as alloying elements. In order to better understand the corrosion behavior of these alloys, we obtained additional information mainly via X-ray photoelectron spectroscopy (XPS) and inductively coupled plasma mass spectroscopy (ICP) techniques. We believe that by studying the corrosion behavior of these alloys after long-term instead of short-term immersion, the latter of which is very often reported in the literature, we bring added value to the study because more accurate information about their corrosion behavior is gained.

2. Materials and Methods

The alloys used in this study are commercial ones (i.e., System NE-Co21Cr8Mo7W; Co29Cr7W—System Soft) and were obtained from Adentatec (Köln, Germany) in the cast state. The nominal composition of these alloys is presented in Table 1. Both materials were tested in the form of rods 8 mm in diameter.

Table 1. Nominal chemical composition (% wt.) of the main components of Co21Cr8Mo7W and Co29Cr7W alloys.

Sample	% Co	% Cr	% Mo	% W
Co21Cr8Mo7W	64	21	8	7
Co29Cr7W	64	29	-	7

Before the experiments, the samples were mechanically prepared by grinding with abrasive paper and suspensions of micrometric alumina powder up to the metallographic quality. They were then degreased in ethanol in an ultrasonic bath and rinsed with distilled water.

The experiments were performed in a 0.1 M phosphate buffer saline solution (PBS) with the following composition: 8 gL^{-1} NaCl, 0.2 gL^{-1} KCl, 1.44 gL^{-1} Na_2HPO_4 and 0.25 gL^{-1} KH_2PO_4. The solution was maintained at a pH of 7.4 and a temperature of 37 °C. All reagents were analytical-grade (Sigma-Aldrich), and the solution was prepared using bidistilled water.

2.1. Electrochemical Measurements

The open-circuit potential was monitored during 1000 h of immersion at 37 °C in naturally aerated solutions, and the potential values are related to Ag/AgCl reference electrode. Three identical samples of 1 cm^2 were immersed in a 50 mL PBS solution in a Thermocal 20 incubator. At predetermined intervals, the stationary potentials were measured in open circuit (OCP). After different periods of immersion (168 and 1000 h), the Tafel curves were recorded in a potential range of 250 mV vs. Ag/AgCl around the corrosion potential, with a rate of 2.5 mV s^{-1} to evaluate the corrosion rate of the specimen. The corrosion parameters i_{cor}, E_{cor} and R_{cor} were extracted from the polarization curves using CorrView 2.3 software through Tafel slope extrapolation.

At the same time, the EIS data acquired potentiostatic at-rest potential between 1 MHz and 10^{-2} Hz, with a perturbation of 10 mV. At the end of the immersion period, the anodic polarization curves were acquired between −300 mV and +1000 mV, with a potential sweep rate of 2.5 mVs^{-1}. All electrochemical measurements were performed using a PARSTAT 4000 potentiostat/galvanostat in a three-electrode electrochemical cell with a platinum sheet as a counter electrode, Ag/AgCl as a reference electrode and the samples as a working electrode. The acquired data were processed using CorrView 3.3d and Zview 2.70 dedicated software. To ensure the reproducibility of the results, three identical samples of each alloy (Co21Cr8Mo7W and Co29Cr7W) were tested.

2.2. Surface Characterization and Electrolyte Analysis

The surface chemical compositions of these alloys were investigated by X-ray Photoelectron Spectroscopy (XPS) using an Escalab Xi+ system from Thermo Scientific (East Grinstead, UK) with an Al Ka gun. Acquisition steps of 1 eV and 0.1 eV were used for general spectra and high-resolution spectra, respectively. The deconvolution of high-resolution spectra was performed using Thermo Scientific Avantage Software v5 9921 (East Grinstead, UK). The C1s line at 284.4 eV was used as a reference to correct the binding energies for charge energy shift. A Shirley background was subtracted from the spectra. Least-square curve fitting of the spectra was performed based on a mixture of Gaussian–Lorentzian functions.

The changes in the hydrophobicity of the surface due to deposition of corrosion products were highlighted by wetting analysis. The contact angle measurement was done with a Drop Shape Analyzer System, 133 DSA1 model (FM40 Easy Drop) from KRÜSS (Hamburg, Germany). The samples were placed on a plane support and drops of deionized water with a volume of 3 µL each were placed on the surface with a dispensing micro-syringe. The contact angle values were collected under static conditions at room temperature, first immediately and then at 30 s after the drop of water was placed on the sample surface. The static contact angle was recorded using the sessile drop fitting method for the angles between 30–90°, and the circle fitting method was used for angles less than 30°. Over 7 measurements were averaged for each sample.

The surface characterization of samples before and after immersion consisted of morphological analysis of the surface of samples at low and high magnifications by scanning electron microscopy using an FEI F50 Inspect SEM (FEI Company, Brno, Czech Republic). The morphology of the film that formed was investigated via secondary electron images (ETD detector—Everhart Thornley Detector, FEI Company) at both low and high magnifications.

The chemical analysis of electrolytes after 168 h of immersion was performed using an inductively coupled plasma optical emission spectrometer with axial and radial viewing plasma configuration (ICP-OES, Optima 2100 DV Perkin Elmer) operating at a 40 MHz free-running ratio-frequency. For each extraction environment, two blank samples were measured as a reference.

3. Results and Discussions

3.1. Electrochemical Evaluation of CoCrMoW Alloys

The electrochemical characterization of Co21Cr8Mo7W and Co29Cr7W samples was carried out in order to analyze the corrosion behavior of these alloys in PBS.

3.1.1. OCP Evolution

Figure 1 presents the results of OCP monitoring over time for both alloys when they were immersed in PBS solution for 1000 h at 37 °C. The evolution of the OCP with time is almost the same for both samples. During the first 24 h, the initial potentials increase significantly at an approximative rate of 7.7 mV h^{-1} (up to +50 mV for Co21Cr8Mo7W and −50 mV for Co29Cr7W), indicating the spontaneous formation of a protective layer on the surfaces of the materials in the biofluid. For both samples, between 24 and 230 h of immersion, the OCP values change over time, suggesting that some processes of adsorption or/and dissolution are occurring at the interface, leading inevitably to both surface-composition changes and apparently to slight instability of the protective layer. According to data from the literature [21,22], among the possible processes of adsorption/dissolution that could occur at the interface, the adsorption of the phosphate ions on the alloy surface (mainly as chromium- and cobalt-phosphate complexes (e.g., $Co(H_2PO_4)_2$), followed by the partial dissolution of these complexes, is one possibility. As other reports suggest [9,21,23], the formation of these chromium and cobalt phosphate species on the surface might mitigate corrosion attack. Indeed, this phenomenon was observed in our case. Thus, as Figure 1 illustrates, the OCP values remain approximately constant between

230 and 1000 h, revealing that during this period of immersion, the layer formed on both samples became stable, with protective anti-corrosion properties. However, the OCP values of the Co21Cr8Mo7W alloy are more positive compared to those of the Co29Cr7W alloy, with a difference of 100 mV, regardless of the immersion period (Figure 1). One may infer that the protective layer formed on the surface of Co21Cr8Mo7W confers better protection against further dissolution of the alloys and increases the corrosion resistance of the material [13].

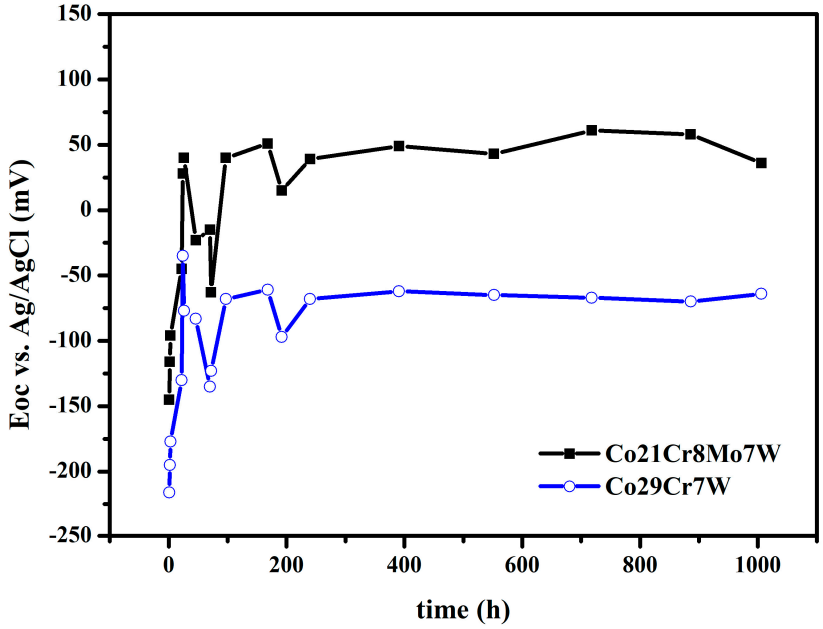

Figure 1. OCP evolution of Co21Cr8Mo7W and Co29Cr7W alloys in 0.1 M PBS solution during 1000 h of immersion at 37 °C.

3.1.2. Anodic Polarization

In order to obtain more information about corrosion behavior of both samples, after 1000 h of immersion in PBS, the Tafel plots and potentiodynamic polarization curves were recorded. They are shown in Figure 2. From the polarization curves, for both samples, a current density (j) less than 10 μA cm^{-2} was observed in a potential range of about 630 mV (Figure 2). These results demonstrate that both samples have a comparable domain of passivation in which the film formed on the surface protects the surface against corrosion attack. These findings appear to show that both types of alloys can be used successfully for biomaterial applications because the potential domain in which the dissolution of the oxide layer is impeded is quite large. For other CoCrMo alloys, a similar domain of passivation was seen [9,10,21]. Literature reports attest that the resistance to passive dissolution of CoCr-based alloys is mainly due to the formation of chromium oxide and cobalt and chromium phosphate complexes [10,20,22] on the surface of the material. Given that the chemical composition of our samples is not too different from that of previously studied CoCrMo alloys, one may presume that a similar phenomenon takes place in our case. After 0.6 V vs. Ag/AgCl, a transpassive domain is observed, regardless of the type of specimen, revealing that at the surface of both samples, dissolution of the film starts to occur. One may presume that the attack at the surface after 0.6 V in this neutral environment is most probably results mainly from the dissolution of both chromium oxide and phosphate chromium ion complexes formed on the surface and from water oxidation [10]. The existence of a transpassive domain after 0.6 V was also reported for other cast cobalt-chromium alloys [9,24]. However, as Figure 2 illustrates, in the transpassive domain, a slight increase in the current density (j), i.e., from 10 μA cm^{-2} to 43 μA cm^{-2}, is seen for Co21Cr8Mo7W samples whereas, for Co29Cr7W samples, a sudden increase in the current density, i.e., from 10 μA cm^{-2} to 550 μA cm^{-2}, is observed. This behavior clearly

demonstrates that the layer formed on the Co21Cr8Mo7W surface has better protective properties against corrosion attack and is more stable compared to that on the Co29Cr7W surface. At first, this result appears surprising because the Co29Cr7W alloy, which contains a greater amount of chromium compared to Co21Cr8Mo7W (Table 1), has slightly lower corrosion resistance. In most cases, for different cast CoCrMo alloys [11,25], the presence of a high amount of chromium, mainly as Cr_2O_3, inhibits surface corrosion. Based on these observations, we assume that, in our case, not necessarily the presence of a higher amount of Cr in the alloy brings about better stability of the film and rather, the synergetic effect of Cr, Mo and W present in the alloy prevents the corrosion attack, most probably due to the formation of a very stable and compact layer on the surface of the material. Because it has been observed that the presence of Mo facilitates the formation of a compact and stable chromium oxide film in other CoCrMo alloys, our findings are in line with published results [16,17].

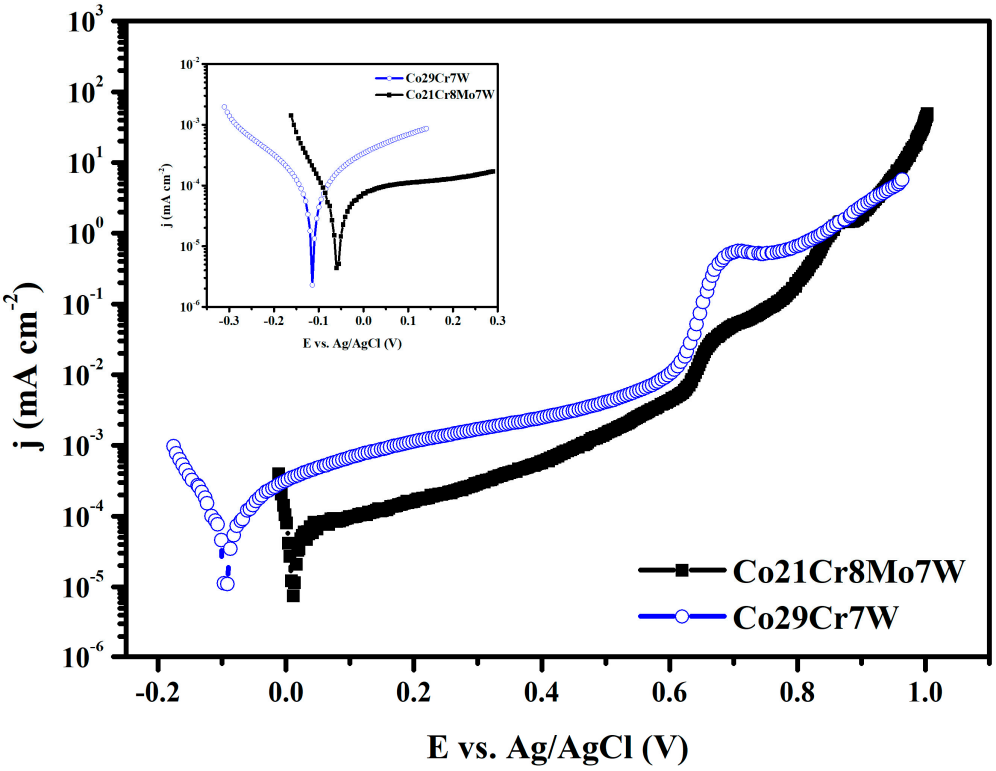

Figure 2. Polarization curves of Co21Cr8Mo7W and Co29Cr7W alloys after 1000 h of immersion in PBS solution at 37 °C. Inset: Tafel plots on Co21Cr8Mo7W and Co29Cr7W alloys after 1000 h of immersion.

In order to gain insight into the corrosion behavior of these alloys with the aim of using them in medical applications, ion-release investigations were performed on both samples after 168 h of immersion according to ISO 10271:2001 [26]. The results, shown in Table 2, reveal that a significant quantity of chromium ions i.e., 73.7 μg cm^{-2}, was released from Co29Cr7W compared to Co21Cr8Mo7W, from which a negligible amount of chromium ions, i.e., 0.15 μg cm^{-2}, was released.

These results are of great importance in terms of the medical applications of these types of alloys because they clearly demonstrate that only Co21Cr8Mo7W is suited for surgical implants (i.e., 0.15 μg cm^{-2} concentration of chromium ion released), as the concentration of chromium ions released is much lower than the level accepted worldwide. (i.e., maximum 0.5 μg cm^{-2} [27]).

Moreover, more chromium ions were observed to be released from Co29Cr7W compared to Co21Cr8Mo7W, mainly in association with the dissolution of chromium oxide or

chromium hydroxide from the passive film. Lower stability of the film on Co29Cr7W is hence expected.

Table 2. Ions released from Co21Cr8Mo7W and Co29Cr7W alloys after 168 h immersion in 0.1M PBS at 37 °C.

Sample	Metal Element	Quantity of Ions Released ($mg\ L^{-1}$)	($\mu g\ cm^{-2}$)
Co21Cr8Mo7W	Co	0.679 ± 0.2	7.1 ± 2
	Cr	$<0.02 \pm 0.01$	0.15 ± 0.1
	Mo	0.021 ± 0.01	0.22 ± 0.1
	W	undetectable	
Co29Cr7W	Co	0.335 ± 0.1	3.33 ± 1.1
	Cr	7.40 ± 0.7	73.7 ± 1.5
	W	undetectable	

This corrosion behavior of our CoCrMoW alloys deserves further detailed investigation to verify that Co21Cr8Mo7W is more appropriate for biomaterials applications and to elucidate the main factors responsible for such behavior.

Better protective properties of the film formed on Co21Cr8Mo7W against corrosion processes were also clearly shown by the corrosion parameters (Table 3), as estimated from Tafel plots (inset Figure 2). Therefore, the corrosion potentials (E_{cor}) determined after two different period of immersion are more positive (Table 3) for Co21Cr8Mo7W, i.e., −0.061 V and −0.059 V at 168 and 1000 h of immersion for Co21Cr8Mo7W and −0.104 V and −0.114 V for Co29Cr7W at the same immersion times. Furthermore, the corrosion current density (j_{cor}), as determined after the same immersion times, is lower (Table 3) for Co21Cr8Mo7W, i.e., 0.038 μA cm^{-2} and 0.049 μA cm^{-2} for Co21Cr8Mo7W and 0.427 μA cm^{-2} and 0.180 μA cm^{-2} for Co29Cr7W. As expected, a similar trend was observed for the evolution of the corrosion rate, measured at the same periods of immersion, where slower corrosion rates were observed for Co21Cr8Mo7W, i.e., 1.09 μm y^{-1} and 2.81 μm y^{-1}. From these results, it is also interesting that the corrosion parameters of Co21Cr8Mo7W, i.e., E_{cor}, i_{cor} and corrosion rates, do not change noticeably with immersion time, revealing that the protective film formed on the CoCrMoW alloy remains stable. One may conclude that Co21Cr8Mo7W has better corrosion resistance and is more appropriate for surgical applications.

Table 3. Corrosion parameters of Co21Cr8Mo7W and Co29Cr7W alloys after immersion in 0.1 M PBS at 37 °C.

Sample	i_{cor}· ($\mu A\ cm^{-2}$)		E_{cor} vs. Ag/AgCl (mV)		Corrosion Rate ($\mu m\ y^{-1}$)	
	168 h	1000 h	168 h	1000 h	168 h	1000 h
Co21Cr8Mo7W	0.038 ± 0.02	0.049 ± 0.02	-61 ± 5	-59 ± 5	1.09 ± 0.5	2.81 ± 0.6
Co29Cr7W	0.427 ± 0.12	0.180 ± 0.15	-104 ± 10	-114 ± 10	12.24 ± 0.7	6.57 ± 0.7

In terms of medical applications, another property of these materials that should not be disregarded is their hydrophobic/hydrophilic character, which is influenced by the protective film formed on the surface of the samples. Therefore, the static contact angles were measured before and after 1000 h of immersion for both specimens. The results revealed that for both types of samples, the character of sample surface changed from hydrophobic before the immersion (i.e., 99.33 ± 0.5 dgr for Co21Cr8Mo7W and 98.93 ± 0.5 dgr for Co29Cr7W) to hydrophilic after the immersion (i.e., 69.87 ± 0.5 dgr for Co21Cr8Mo7W and 67.79 ± 0.5 dgr for Co29Cr7W), suggesting that the protective film formed on both types of alloys is hydrophilic. Therefore, the evidence that a hydrophilic stable layer forms on these

alloys and subsequently both inhibits corrosive attack and provides a surface with good affinity for the adhesion of cells might open up new possibilities for obtaining CoCrMoW alloys with beneficial properties for medical implants.

3.2. Electrochemical Impedance Spectroscopy

Additional information about the corrosion behavior of both types of samples was obtained from the EIS investigations, which were carried out potentiostatically at OCP after 1000 h of immersion in PBS solution.

As Figure 3a illustrates, within the frequency range from 0.01 to 10^5 Hz, the impedance Z is much higher for Co21Cr8Mo7W compared to Co29Cr7W, suggesting that the oxide film formed on Co21Cr8Mo7W exhibits better protective anti-corrosion properties. These findings are in good agreement with previous ones from anodic polarization investigations, which revealed similar corrosion behavior in both samples.

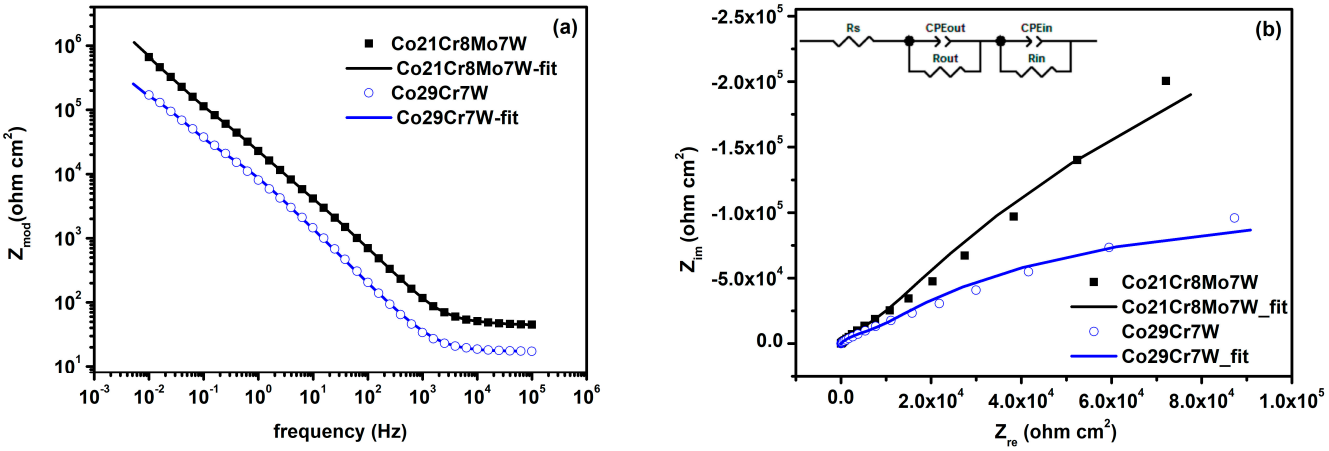

Figure 3. Bode plots (**a**) and Nyquist diagrams (**b**) of Co21Cr8Mo7W and Co29Cr7W alloys with their simulated curves (solid line) after 1000 h of immersion in PBS at 37 °C. Inset: the equivalent circuit.

In order to gain further information about the corrosion behavior of these samples, the impedance spectra of both specimens (Figure 3) were fitted by considering an equivalent circuit (EEC) with two time constants in series (Figure 3b, inset). Using this EEC, the experimental data gave the best fit. The first time constant, constituted from CPE_{in}/R_{in}, is attributed to the oxide layer formed on the surface during the immersion, and the second time constant, constituted from CPE_{out}/R_{out}, accounts for the dissolution processes at the alloy/electrolyte interface and the inhomogeneity of the passive film. Due to these complex physical phenomena and to the heterogeneity of the surface, the constant-phase elements (CPE_{out} and CPE_{in}) were more suitable than the capacitances for fitting the EIS spectra [28] and the chi-squared values (X^2) are less than 1.3×10^{-3} for both samples. This EEC has previously been successfully used for describing the corrosion behavior of other CoCrMo alloys in different media [9,10,12]. The values of the equivalent circuit parameters of both alloys in the PBS solution are shown in Table 4.

Table 4. EIS parameters obtained from fitting experimental data on the proposed equivalent electrical circuit of Co21Cr8Mo7W and Co29Cr7W alloys after 1000 h of immersion in 0.1M PBS at 37 °C.

Sample	Rs (Ω cm^2)	$CPE_{out} \times 10^{-5}$ ($S^n\ \Omega^{-1}$ cm^{-2})	n	R_{out} (Ω cm^2)	$CPE_{in} \times 10^{-5}$ ($S^n\ \Omega^{-1}$ cm^{-2})	n	$R_{in} \times 10^6$ (Ω cm^2)
Co21Cr8Mo7W	15.78 ± 0.8	5.63 ± 0.24	0.80 ± 0.02	6461 ± 70	3.85 ± 0.35	0.81 ± 0.02	8.6 ± 0.8
Co29Cr7W	17.01 ± 0.7	3.63 ± 0.25	0.86 ± 0.01	7540 ± 60	4.36 ± 0.33	0.84 ± 0.01	2.3 ± 0.5

From these parameters, the polarization resistance (R_p) of both specimens, calculated as the sum of R_{out} and R_{in}, was estimated and they are 8.6×10^6 Ω cm^2 and 2.3×10^6 Ω cm^2 for Co21Cr8Mo7W and Co29Cr7W, respectively. As the R_p values of both samples are on the order of Megaohms, it appears that the film formed on both specimens has good corrosion resistance and, from this perspective, they can be used for surgical applications. However, the R_p of the Co21Cr8Mo7W alloy is approximately four times higher than that of the Co29Cr7W alloy, suggesting that a more stable oxide film with better corrosion resistance is formed on Co21Cr8Mo7W. These results are in good agreement with electrochemical corrosion investigations that confirmed the superior corrosion performance of the Co21Cr8Mo7W alloy and a lower rate of passive-layer dissolution (Table 3). These findings are supported by the results obtained for the inner resistances (R_{in}) of both samples, which seem to suggest a similar trend (Table 4). The EIS results point out clearly that the Co21Cr8Mo7W alloy has better surface protection.

3.3. X-ray Photoelectron Spectroscopy Investigations

The surface chemical composition of the Co21Cr8Mo7W and Co29Cr7W alloys was investigated by XPS after their immersion in PBS solution at 37 °C for 1000 h. The XPS analysis revealed mainly the presence of cobalt, chrome, tungsten, oxygen and phosphorus on the surfaces of both specimens. Additionally, on the Co21Cr8Mo7W surface, molybdenum is observed. These results are in line with those from the chemical-composition analysis (Table 1), which revealed the presence of the cobalt, chromium and tungsten elements in the bulk of both types of alloys and molybdenum only in the Co21Cr8Mo7W bulk alloy.

Based on literature reports [9,13] and on our findings, which revealed the presence of a certain amount of phosphorus (i.e., cca. 18%) on the surface of both specimens, one may assume that during immersion, a non-negligible quantity of cobalt- and chromium-phosphate complexes (e.g., $Co(H_2PO_4)_2$) are formed on the surface. The presence of these adsorbed complexes on the protective film formed on alloys, as the electrochemical results suggest, is expected to mitigate the corrosion attack and hence to contribute to ensuring a large passivation domain for both alloys, i.e., about 630 mV.

In order to better understand the corrosion behavior of these alloys, the high-resolution spectra of Cr 2p, W 4f, Mo 3d and O 1s were recorded. The deconvoluted high-resolution spectra of both alloys are shown in Figures 4 and 5.

The Cr-2$p_{3/2}$ spectra of both types of alloys were fitted with 5 peaks (Figures 4a and 5a). These peaks are attributed to chromium metallic species (Cr^0) (BE 547.5 ± 0.2 eV, [13,18]); Cr (III) oxide, most probably present as Cr_2O_3 species (BE = 575.7 ± 0.2 eV, [13,16]); $Cr(OH)_3$ species (BE 576.9 ± 0.2 eV, [13,16]); mixed-oxide chromium species (BE 578.2 ± 0.2 eV, [29]); and Cr (VI) oxide, like CrO_3 species (BE 579.5 ± 0.2 eV, [23]). The corresponding relative fractions of the chemical species are shown in the figure insets. From the deconvoluted Cr-2$p_{3/2}$ spectra, one may conclude that a significant quantity of Cr_2O_3 and $Cr(OH)_3$ species are formed on the surfaces of both specimens. It is well known that the presence of these constituents in the passive film ensures that the film will have good protective anti-corrosion properties [9,13,16]. Thus, based on these findings, one may presume that the good protective properties of the films formed on the surface of both alloys are due to the presence of these non-negligible amounts of chromium oxide and chromium hydroxide species in the films. However, a higher concentration of Cr_2O_3 and $Cr(OH)_3$ species is present in the passive film formed on the Co29Cr7W surface (i.e., Cr_2O_3 20.29% and $Cr(OH)_3$ 30.90%) compared to that on the surface of Co21Cr8Mo7W (i.e., Cr_2O_3 14.91% and $Cr(OH)_3$ 28.52%). These results, along with those from electrochemical investigations, suggest that the presence of a greater amount of Cr_2O_3 and chromium hydroxide species in the film does not necessarily guarantee that the film will have improved protective anti-corrosion properties. Therefore, in order to provide a more comprehensive understanding of the corrosion behavior of these alloys, further XPS analysis was necessary.

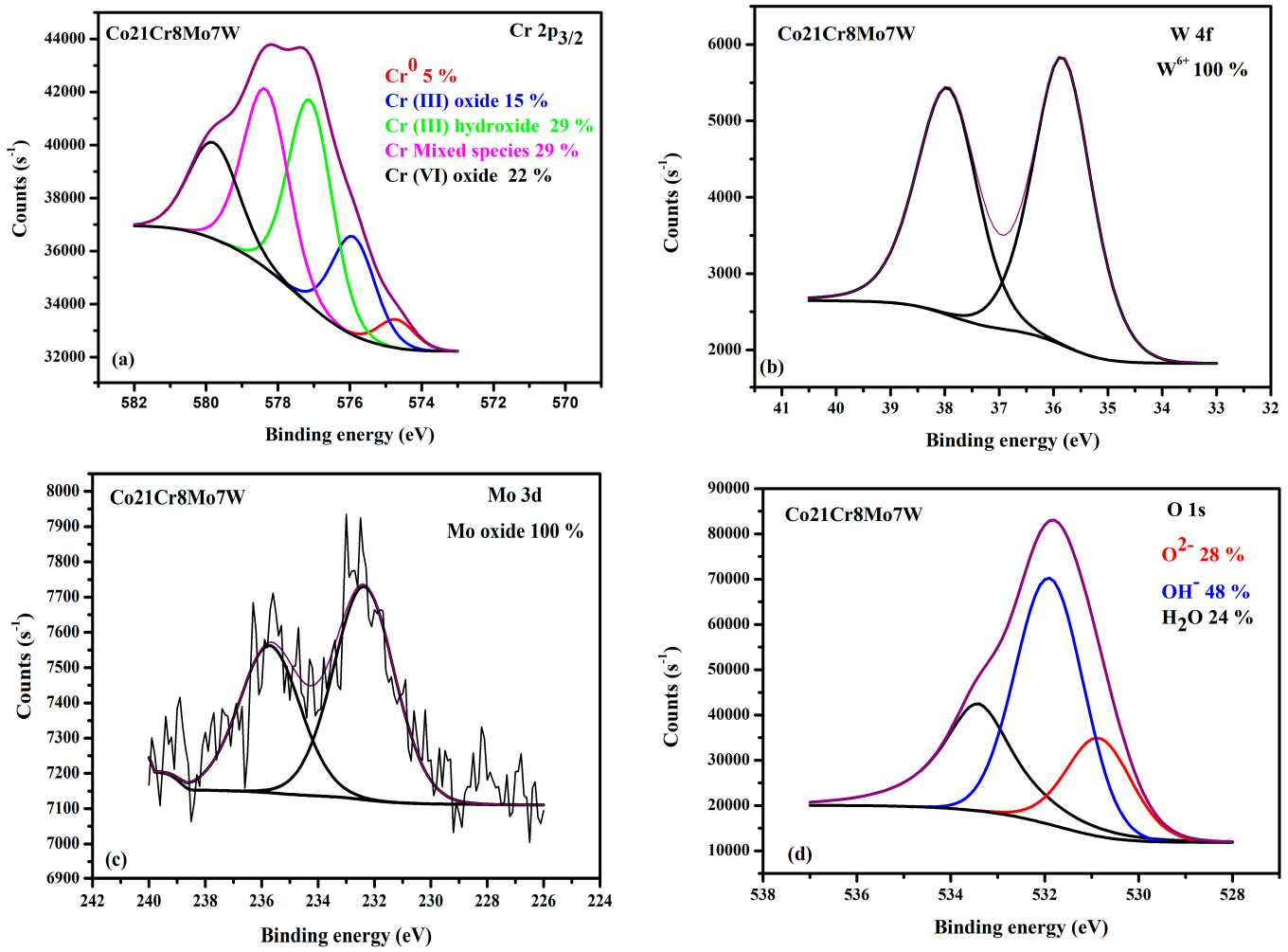

Figure 4. High-resolution XPS spectra recorded in the: (**a**) Cr $2p_{3/2}$, (**b**) W 4f, (**c**) Mo 3d and (**d**) O 1s regions for the Co21Cr8M7W alloy.

The W-4f spectra of Co21Cr8Mo7W were deconvoluted by assuming one doublet associated with WO_3 species (the W $4f_{7/2}$ of this doublet is at BE 35.9 eV ± 0.2 eV, [30,31]) (Figure 4b), and W-4f spectra of Co29Cr7W (Figure 5b) were deconvoluted by assuming three doublets attributed to W^0 species (the W $4f_{7/2}$ of the first doublet is at BE 31.4 ± 0.2 eV, [30,31]), W^{5+} species (the W $4f_{7/2}$ of the second doublet is at BE 34.9 ± 0.2 eV, [32]) and WO_3 species (the W $4f_{7/2}$ of the third doublet is at BE 36 ± 0.2 eV [30,31]). For each doublet, we considered a spin-orbit splitting of 2.1 eV and a W $4f_{7/2}$/W $4f_{5/2}$ ratio of 1.33 [32]. The corresponding relative fractions of the chemical species are shown in the insets of the corresponding figures. These results clearly demonstrate that the tungsten constituent in the protective film formed on the Co21Cr8Mo7W surface is present only as tungsten (VI) oxide species, whereas on the Co29Cr7W surface, it is also present as W metallic and W^{5+} species.

As to the Mo 3d spectrum of Co21Cr8Mo7W, this spectrum was deconvoluted by considering one doublet to be associated with MoO_3 species (the Mo $3d_{5/2}$ of this doublet is at 232.7 ± 0.2 eV, [22,29]) (Figure 4c). For this doublet, we considered a spin-orbit splitting of 3.13 eV and a Mo $3d_{5/2}$/Mo $3d_{3/2}$ ratio of 0.67 [29]. It is clear from these results that the molybdenum constituent in the film is present only as MoO_3.

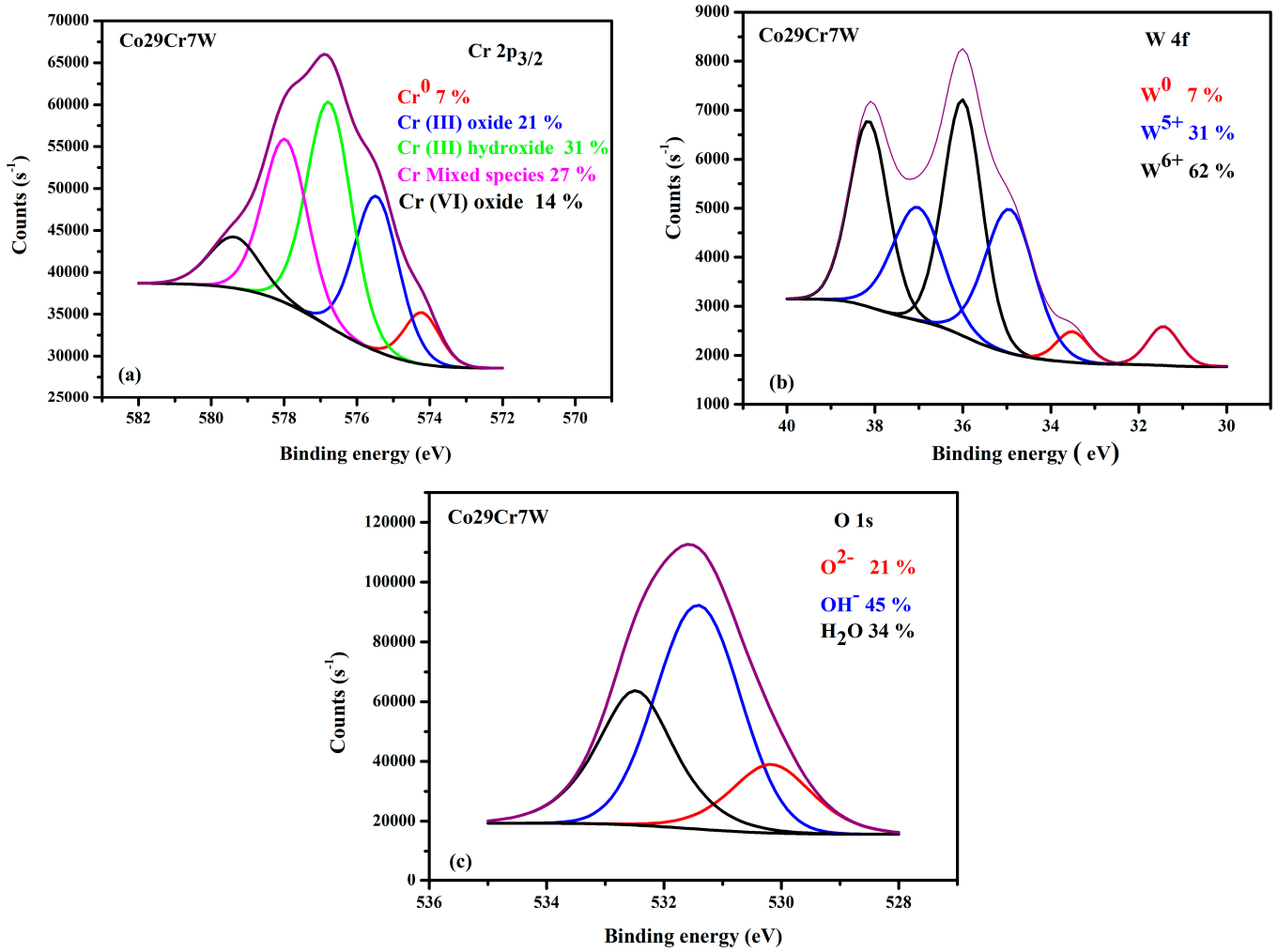

Figure 5. High-resolution XPS spectra recorded in the: (**a**) Cr $2p_{3/2}$, (**b**) W 4f and (**c**) O 1s regions for the Co29Cr7W alloy.

In summary, from the above XPS investigations and literature data [11,18,20], one may conjecture that the good corrosion resistance observed for Co29Cr7W alloys results from the presence in the passive film of both chromium species (i.e., Cr_2O_3 and $Cr(OH)_3$) in significant amounts and of tungsten oxide species in a much lower amount. Conversely, for Co21Cr8Mo7W, the XPS results, in correlation with reported data [16,17,19], revealed that the good corrosion behavior of this alloy is mainly due to the synergetic effect of Cr, W and Mo, which are present in the film as Cr_2O_3, $Cr(OH)_3$, WO_3 and MoO_3. Previous data from the literature [16,33] revealed that better corrosion resistance of the film formed on CoCr-based alloy surfaces might be obtained when Mo and W are incorporated as alloying elements. The addition of Mo has been observed to enhance resistance to pitting corrosion through the facilitation of passive-film formation, while the incorporation of W strengthens the structural and chemical stability of the alloy [34,35]. The MoO_x and WO_3 species present in the passive film seem to ensure good compactness of the film [33]. Other reports [16] have demonstrated that an efficient barrier against the diffusion of species through the film formed on the surface of these types of alloys might be obtained when both MoO_2/similar products and WO_3 are present in the protective oxide film. It was also evidenced that these oxide species contribute to slowing the selective dissolution of the metals beneath them.

As a conclusion, based on the XPS results and electrochemical outcomes, one may emphasize that the better corrosion performance observed for the Co21Cr8Mo7W alloy

is strongly related to the synergetic effects of Cr, W and Mo and therefore should not be disregarded.

These observations are noteworthy because they establish that the presence of greater amounts of Cr in the alloy (i.e., 29% for Co29Cr7W and 21% for Co21Cr8Mo7W) does not necessarily strongly impede corrosion processes (i.e., R_{cor} is 2.81 μm y^{-1} for Co29Cr7W and 1.09 μm y^{-1} for Co21Cr8Mo7W). In fact, the synergetic effect of Cr, Mo and W constituents present in the passive film as oxides is responsible for excellent protective properties of the film against corrosion attack. In other words, it is possible that, in our case, for Co21Cr8Mo7W, the presence of W as only hexavalent tungsten oxide and of molybdenum as MoO_3 in the film improves the protective properties of the passive film, thus more strongly impeding dissolution processes in the film. Furthermore, Cwalina K.L. et al. [17] demonstrated that the presence of WO_3 species in the passive film extends the passive range because the stability of the film is enhanced by means of the interaction of W with water, which leads to the formation of the insoluble WO_3 phase. Thus, we consider that the extended passive range and lowered passive current density observed for the Co21Cr8Mo7W alloy (i.e., ΔE_{pass} = 0.63 V; i_{pass} = 0.4 μA cm^{-2}) compared to the Co29Cr7W alloy (ΔE_{pass} = 0.49 V; i_{pass} = 1.2 μA cm^{-2}) is also due to the presence of a greater quantity of WO_3 species in the passive film formed on the Co21Cr8Mo7W surface (Figures 4b and 5b).

The O-1s spectra of both types of alloys, deconvoluted with three peaks associated with $O^{metal\text{-}oxide}$ species (BE 530.4 ± 0.2 eV, [9,13]), hydroxide or hydroxyl groups, OH^- (BE 531.7 ± 0.2 eV, [36]) chemisorbed water (BE = 532.8 ± 0.3 eV, [36] and/or metal-PO_4 [23] (Figures 4d and 5c), support our above XPS results, which attest mainly the presence of oxygen bonded to the metal and the formation of $Cr(OH)_3$.

The corresponding relative fractions of the chemical species are shown in the insets of Figures 4d and 5c.

Moreover, as the O-1s spectra reveal, a non-negligible quantity of hydroxide or hydroxyl groups is present. For example, $Cr(OH)_3$ is present on the surfaces of both specimens, (i.e., around 46% OH^- species, no matter the type of sample, Figures 4d and 5c). The presence of a considerable quantity of these types of species on the surface of both alloys is of great importance because these species may contribute significantly to the hydrophilic character of the surface, as evidenced by static contact angle measurements. The hydrophilic character of the surface, in terms of surface affinity for the adhesion of the cells, is indispensable for medical applications.

One may conclude that in terms of medical applications, this strategy of adding W and Mo as alloying elements to the CoCr alloy is of great perspective in obtaining CoCr-based alloys with a lower content of chromium than is usually used for such applications.

3.4. Microstructure and Surface Morphology

The surface samples were investigated by SEM without etching, and Figure 6 illustrates the surface state of the Co21Cr8Mo7W and Co29Cr7W alloys before and after immersion. For image acquisition, relatively lower magnifications were employed to obtain a general view, while higher magnifications were utilized for a more detailed examination. As expected, the surface morphology is relatively similar in both types of samples before immersion, with some differences occurring due to the different levels of metallographic preparation (Figure 6a,c). The SEM investigation indicates that both alloys exhibit characteristic dendritic microstructures with various inclusions and impurities clearly visible in the surface samples after immersion (Figure 6b,d). Furthermore, these microstructures confirm that the direction of solidification during casting was uniform in all directions for both alloys. After immersion, a thin film mirroring the texture of the material and randomly dispersed small particles are detectable on the surface of both types of samples (Figure 6b,d). As previously demonstrated by Lekatou et al. for other Co–Cr–Mo alloys [37], these small particles most likely originate from the interaction between the alloy and PBS. Moreover, notable differences in surface morphology of the samples are observed (Figure 6b, d inset), suggesting that the protective oxide layers formed on the

surfaces of these alloys might exhibit different properties. The passive film appears to be more compact and more uniformly formed on the surface of the Co21Cr8Mo7W alloy (Figure 6b inset). These findings, along with those from electrochemical investigations, seem to reveal that the better corrosion resistance observed for Co21Cr8Mo7W alloy is also the result of the formation of a more uniform and more compact film on this alloy.

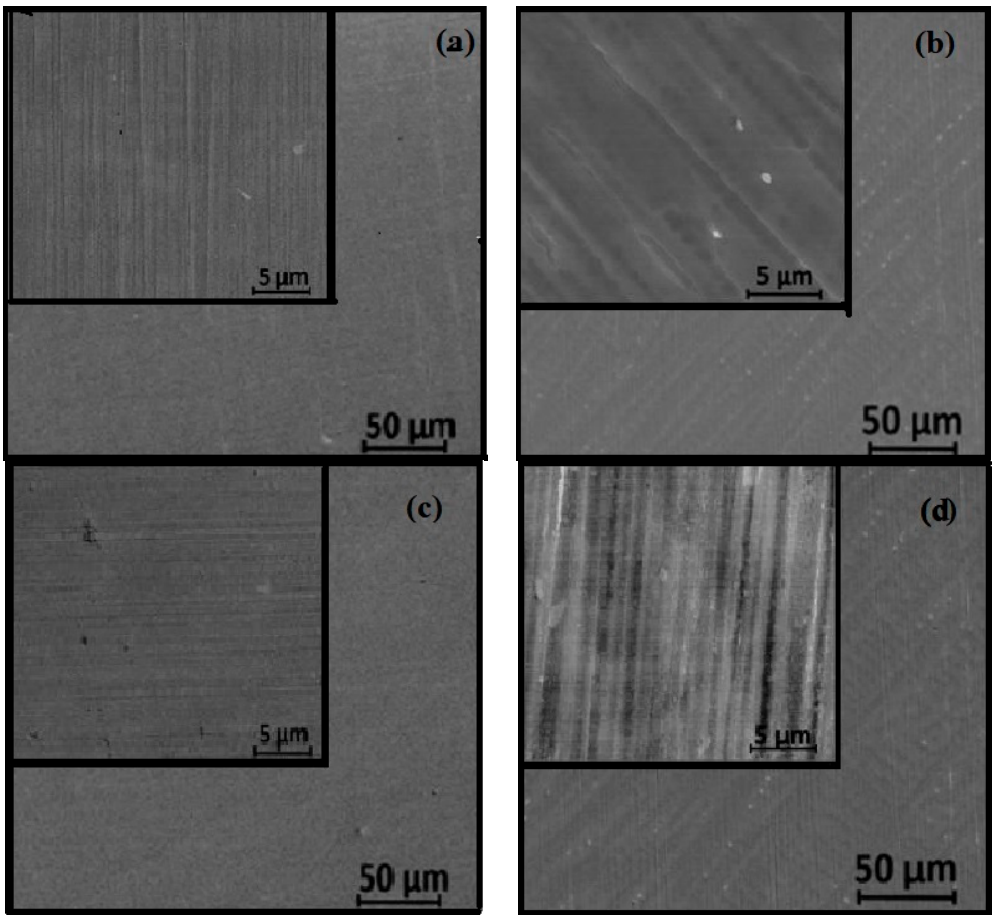

Figure 6. SEM images of the surface of the Co21Cr8Mo7W alloy: (**a**) before and (**b**) after immersion in PBS, and of Co29Cr7W alloy (**c**) before, and (**d**) after 1000 h of immersion in PBS. Inset: magnified view of the surface.

4. Conclusions

The corrosion behavior of two cast CoCr-based alloys, one with a lower content of chromium (Co21Cr8Mo7W) and another with a higher content of chromium (Co29Cr7W), was systematically investigated over the course of a long period of immersion in 0.1 M PBS by electrochemical methods.

After 1000 h of immersion, the anodic polarization curves clearly revealed that both studied alloys present good corrosion resistance. Despite the fact that both alloys have similar corrosion behavior, from the estimation of the corrosion parameters, one may resume that the Co21Cr8Mo7W alloy has better corrosion protection (i.e., i_{cor} = 49 nA cm^{-2}, E_{cor} = −59 mV and R_{cor} = 2.81 µm y^{-1}) than the Co29Cr7W alloy (i.e., i_{cor} = 180 nA cm^{-2}, E_{cor} = −114 mV and R_{cor} = 6.57 µm y^{-1}). This behavior suggests that on the Co21Cr8Mo7W surface, a more stable and compact passive film is formed. These outcomes are in line with EIS results, which evidenced a higher polarization resistance (R_p) for the Co21Cr8Mo7W alloy (i.e., 8.6 M Ω cm^2) compared to the Co29Cr7W alloy, for which an R_p of 3 M Ω cm^2 was determined.

The good corrosion resistance observed for Co29Cr7W, as revealed by the XPS investigations, is mainly due to the presence of chromium species (i.e., Cr_2O_3, $Cr(OH)_3$) and tungsten oxide species in the passive film. For Co21Cr8Mo7W, the XPS results suggest that the excellent corrosion behavior of this alloy mainly results from the synergetic effect of Cr, W and Mo, which are present in the film as Cr_2O_3, $Cr(OH)_3$, WO_3 and MoO_3. Moreover, these investigations revealed that the presence of a higher amount of Cr_2O_3 and chromium hydroxide species in the film does not necessarily result in better corrosion performance in these CoCr-based alloys. In fact, the remarkable corrosion resistance observed in CoCr-based alloys with a lower Cr content, namely Co21Cr8Mo7W, emerges, as stated previously, from the strategy of adding different alloying elements (i.e., Mo and W) to the CoCr alloy.

Additionally, as the ion-release measurements suggest, Co21Cr8Mo7W released a low concentration of chromium ions (i.e., 0.15 μg cm^{-2}), very much beneath the accepted medical value, whereas Co29Cr7W released a high concentration of chromium ions (i.e., 73.7 μg cm^{-2}), very much over the accepted medical value.

These results are promising for medical applications, suggesting that the Co21Cr8Mo7W alloy herein studied could be a viable alternative to new CoCr-based alloys developed for such purposes. One benefit to utilizing this type of alloy for surgical applications is that, with a lower amount of Cr, cost-effective and safe surgical devices with minimal chromium-ion release can be produced. Both the as-prepared and after-immersion states of Co-Cr-Mo-W exhibit significant resistance to corrosion in SBF solution, rendering them suitable for biomedical applications from a corrosion perspective.

Author Contributions: Conceptualization, L.P. and M.M.; methodology, L.P.; formal analysis, C.D.; investigation, S.A.L., C.D., E.I.N., M.E.M., V.S. and A.P.; writing—original draft preparation, L.P.; writing—review and editing, M.M.; supervision, M.M. All authors have read and agreed to the published version of the manuscript.

Funding: This study was performed within the framework of the *Electrochemical preparation and characterization of active materials with predetermined features* research project of the "Ilie Murgulescu" Institute of Physical Chemistry of the Romanian Academy, and founded by Romanian Ministry of Research, Innovation and Digitalization (MCID) through Program 1—Development of the National Research and Development System; Subprogramme 1.2—Institutional performance—Projects financed for excellence in RDI, grant no. 30PFE/2021.

Data Availability Statement: The data presented in this study are available on request from the corresponding author.

Conflicts of Interest: The authors declare that they have no known competing financial interests or personal relationships that could have appeared to influence the work reported in this paper.

References

1. Dobri, G.; Banu, A.; Donath, C.; Marcu, M. The Influence of the Tantalum Content on the Main Properties of the TixTa9Nb8Zr2Ag Alloy. *Metals* **2023**, *13*, 1294. [CrossRef]
2. Wanga, Q.; Eltit, F.; Fenge, R.; Garbuz, D.; Duncan, C.; Masri, B.A.; Greidanus, N.; Coxc, M.E.; Wanga, R. Nature of fretting corrosion products in CoCrMo hip implants from in vivo study to in vitro simulation. *Materialia* **2022**, *22*, 101433. [CrossRef]
3. Acharya, S.; Soni, R.; Suwas, S.; Chatterjee, K. Additive manufacturing of Co–Cr alloys for biomedical applications: A concise review. *J. Mater. Res.* **2021**, *36*, 3746–3760. [CrossRef]
4. Mazumder, S.; Man, K.; Radhakrishnan, M.; Pantawane, M.V.; Palaniappan, S.; Patil, S.M.; Yang, Y.; Dahotre, N.B. Microstructure enhanced biocompatibility in laser additively manufactured CoCrMo biomedical alloy. *Biomater Adv.* **2023**, *150*, 213415. [CrossRef] [PubMed]
5. Mace, A.; Khullar, P.; Bouknight, C.; Gilbert, J.L. Corrosion properties of low carbon CoCrMo and additively manufactured CoCr alloys for dental applications. *Dent. Mater.* **2022**, *38*, 1184–1193. [CrossRef]
6. Yan, Y.; Neville, A.; Dowson, D.; Williams, S. Tribocorrosion in implants—Assessing high carbon and low carbon Co–Cr–Mo alloys by in situ electrochemical measurements. *Tribol. Int.* **2006**, *39*, 1509. [CrossRef]
7. España, F.A.; Balla, V.K.; Bose, S.; Bandyopadhyay, A. Design and fabrication of CoCrMo alloy based novel structures for load bearing implants using laser engineered net shaping. *Mater. Sci. Eng. C* **2010**, *30*, 50–57. [CrossRef]
8. Yamanaka, K.; Mori, M.; Kuramoto, K.; Chiba, A. Development of new Co-Cr-E based biomedical alloys: Effects of micro alloying and thermo mechanical processing on microstructures and mechanical properties. *Mater. Des.* **2014**, *55*, 987–998. [CrossRef]

9. Igual, M.A.; Mischler, S. Interactive Effects of Albumin and Phosphate Ions on the Corrosion of CoCrMo Implant Alloy. *J. Electrochem. Soc.* **2007**, *154*, C562–C570. [CrossRef]
10. Vidal, V.C.; Igual, M.A. Effect of physico-chemical properties of simulated body fluids on the electrochemical behaviour of CoCrMo alloy. *Electrochim. Acta* **2011**, *56*, 8239–8248. [CrossRef]
11. Banu, A.; Marcu, M.; Juganaru, C.; Osiceanu, P.; Anastasescu, M.; Capra, L. Corrosion behavior of CoCrMoW cast alloy in lactic environment. *Arab. J. Chem.* **2019**, *12*, 2007–2016. [CrossRef]
12. Metikos-Hukovic', M.; Pilic´, Z.; Babic´, R.; Omanovic, D. Influence of alloying elements on the corrosion stability of CoCrMo implant alloy in Hank's solution. *Acta Biomater.* **2006**, *2*, 93–700. [CrossRef] [PubMed]
13. Milosev, I.; Strehblow, H.-H. The composition of the surface passive film formed on CoCrMo alloy in simulated physiological solution. *Electrochim. Acta* **2003**, *48*, 2767–2774. [CrossRef]
14. Garcia-Falcon, C.M.; Gil-Lopez, T.; Verdu-Vazquez, A.; Mirza-Rosca, J. Electrochemical characterization of some cobalt base alloys in Ringer solution. *Mater. Chem. Phys.* **2021**, *260*, 124164. [CrossRef]
15. Wang, R.; Qin, G.; Zhang, E. Hot deformation characteristics and dynamic recrystallization of biomedical CoCrWCu alloy. *Mater. Today Commun.* **2022**, *33*, 104930. [CrossRef]
16. Tian, W.-P.; Yang, H.-W.; Zhang, S.-D. Synergistic Effect of Mo, W, Mn and Cr on the Passivation Behavior of a Fe-Based Amorphous Alloy Coating. *Acta Metall. Sin. (Engl. Lett.)* **2018**, *31*, 308–320. [CrossRef]
17. Cwalina, K.L.; Demarest, C.R.; Gerard, A.Y.; Scully, J.R. Revisiting the effects of molybdenum and tungsten alloying on corrosion behavior of nickel-chromium alloys in aqueous corrosion. *Curr. Opin. Solid State Mater. Sci.* **2019**, *23*, 129–141. [CrossRef]
18. Gurel, S.; Nazarahari, A.; Canadinc, D.; Gerstein, G.; Maier, H.J.; Cabuk, H.; Bukulmez, T.; Cananoglu, M.; Yagci, M.B.; Toker, S.M.; et al. From corrosion behavior to radiation response: A comprehensive biocompatibility assessment of a CoCrMo medium entropy alloy for utility in orthopedic and dental implants. *Intermetallics* **2022**, *149*, 107680. [CrossRef]
19. Vidal, V.C.; Igual, M.A. Electrochemical characterisation of biomedical alloys for surgical implants in simulated body fluids. *Corros. Sci.* **2008**, *50*, 1954–1961. [CrossRef]
20. Milosev, I. The effect of biomolecules on the behaviour of CoCrMo alloy in various simulated physiological solutions. *Electrochim. Acta* **2012**, *78*, 259–273. [CrossRef]
21. Hodgson, A.W.E.; Kurz, S.; Virtanen, S.; Fervel, V.; Olsson, C.-O.A.; Mischler, S. Passive and transpassive behaviour of CoCrMo in simulated biological solutions. *Electrochim. Acta* **2004**, *49*, 2167–2178. [CrossRef]
22. Hanawa, T.; Hiromoto, S.; Asami, K. Characterization on of the surface oxide film of a Co-Cr-Mo alloy after being located in quasi-biological environments using XPS. *Appl. Surf. Sci.* **2001**, *183*, 68–75. [CrossRef]
23. Ouerd, A.; Alemany-Dumont, C.; Normand, B.; Szunerits, S. Reactivity of CoCrMo alloy in physiological medium: Electrochemical characterization of the metal/protein interface. *Electrochim. Acta* **2008**, *53*, 4461–4469. [CrossRef]
24. Girao, D.d.C.; Beres, M.; Jardini, A.L.; Filho, R.M.; Silva, C.C.; Siero, A.; Gomes de Abreu, H.F.; Araujo, W.S. An assessment of biomedical CoCrMo alloy fabricated by direct metal laser sintering technique for implant applications. *Mater. Sci. Eng. C Mater. Biol. Appl.* **2020**, *107*, 110305. [CrossRef]
25. Tsustumi, Y.; Doi, H.; Nomura, N.; Ashida, M.; Chen, P.; Kawasaki, A.; Hanawa, T. Surface Composition and Corrosion Resistance of Co-Cr Alloys Containing High Chromium. *Mater. Trans.* **2016**, *57*, 2033–2040. [CrossRef]
26. *ISO 10271*; Dentistry-Corrosion Test Methods for Metallic Materials. ISO: Geneva, Switzerland, 2011.
27. Okazaki, Y.; Gotoh, E. Comparison of metal release from various metallic biomaterials in vitro. *Biomaterials* **2005**, *26*, 11–21. [CrossRef]
28. Jakovljevic, S.; Alar, V.; Ivankovic, A. Electrochemical Behaviour of PACVD TiN-Coated CoCrMo Medical Alloy. *Metals* **2017**, *7*, 231. [CrossRef]
29. Marin, E.; Lanzutti, A.; Rondinella, A.; Sordetti, F.; Magnan, M.; Honma, T.; Yoshida, Y.; Zhu, W.; Pezzotti, G.; Fedrizzi, L. Multi-spectroscopic analysis of high temperature oxides formed on cobalt-chrome-molybdenum alloys. *J. Mater.Res. Technol.* **2022**, *20*, 3061–3073. [CrossRef]
30. Zhang, W.; Qi, Y.; Zhang, L.; Tang, Y.; Qi, C.; Shen, Q.; Ma, Y.; Wang, B. The effect of alloy elements on corrosion and oxidative resistance of W-based alloy films. *Surf. Coat. Technol.* **2022**, *434*, 128165. [CrossRef]
31. Marcu, M.; Preda, L.; Vizireanu, S.; Bita, B.; Mihai, M.A.; Spataru, T.; Acsente, T.; Dinescu, G.; Spataru, N. Enhancement of the capacitive features of WO_3 supported on pristine and functionalized graphite by appropriate adjustment of the electrodeposition regime. *Mater. Sci. Eng. B* **2022**, *277*, 115585. [CrossRef]
32. Vasilopoulou, M.; Soultati, A.; Georgiadou, D.G.; Stergiopoulos, T.; Palilis, L.C.; Kennou, S.; Stathopoulos, N.A.; Davazoglou, D.; Argitis, P. Hydrogenated understoichiometric tungsten oxide anode interlayers for efficient and stable organic photovoltaics. *J. Mater. Chem. A* **2014**, *2*, 1738. [CrossRef]
33. Alexander, M.R.; Thompson, G.E.; Zhou, X.; Beamson, G.; Fairley, N. Quantification of oxide film thickness at the surface of aluminium using XPS. *Surf. Interface Anal.* **2002**, *34*, 485–489. [CrossRef]
34. Leban, M.B.; Kurnik, M.; Kopač, I.; Klug, M.J.; Podgornik, B.; Kosec, T. Differences between 3-D printed and traditionally milled CoCr dental alloy from casted block in oral environment. *Electrochim. Acta* **2023**, *445*, 142066. [CrossRef]
35. Dimitriadis, K.; Lekatou, A.G.; Sfikas, A.K.; Roumpi, M.; Tsouli, S.; Galiatsatos, A.; Agathopoulos, S. Influence of Heat-Treatment Cycles on the Microstructure, Mechanical Properties, and Corrosion Resistance of Co-Cr Dental Alloys Fabricated by Selective Laser Melting. *J. Mate. Eng. Perform.* **2021**, *30*, 5252–5265. [CrossRef]

36. Wagner, C.D.; Riggs, W.M.; Davis, L.E.; Moulder, J.F.; Muilenberg, G.E. *Handbook of X-ray Photoelectron Spectroscopy*; Perkin-Elmer Corporation: Eden Prairie, MN, USA, 1979.
37. Lekatou, A.G.; Emmanouilidou, S.; Dimitriadis, K.; Baikousi, M.; Karakassides, M.A.; Agathopoulos, S. Simulating porcelain firing effect on the structure, corrosion and mechanical properties of Co–Cr–Mo dental alloy fabricated by soft milling. *Odontology* **2023**, 1–18. [CrossRef] [PubMed]